Published in final edited form as:

Cancer Res. 2021 November 15; 81(22): 5666–5677. doi:10.1158/0008-5472.CAN-20-3982.

Matricellular protein WISP2 is an endogenous inhibitor of collagen linearization and cancer metastasis

Jagadeesh Janjanam[1,4], **Glendin Pano**[1,4], **Ruishan Wang**[1], **Benjamin A. Minden-Birkenmaier**[1], **Hannah Breeze-Jones**[1], **Eleanor Baker**[1], **Cecile Garcin**[1], **Georgia Clayton**[1], **Abbas Shirinifard**[1], **Ana Maria Zaske**[2], **David Finkelstein**[3], **Myriam Labelle**[1,*]

[1]Comprehensive Cancer Center, Solid Tumor Program, Department of Developmental Neurobiology, St. Jude Children's Research Hospital, Memphis, TN 38105, USA

[2]Division of Cardiology, Department of Internal Medicine, UTHealth – The University of Texas Health Science Center at Houston, Houston, TX 77054, USA

[3]Department of Computational Biology, St. Jude Children's Research Hospital, Memphis, TN 38105, USA

[4]These authors contributed equally.

Abstract

Collagen remodeling contributes to many physiological and pathological processes. In primary tumors, the linearization of collagen fibers promotes cancer cell invasion and metastasis and is indicative of poor prognosis. However, it remains unknown whether there are endogenous inhibitors of collagen linearization that could be exploited therapeutically. Here, we show that collagen linearization is controlled by two secreted matricellular proteins with antagonistic functions. Specifically, WISP1 was secreted by cancer cells, bound to type I collagen (Col I), and linearized Col I via its cysteine-rich C-terminal (CT) domain. In contrast, WISP2, which lacks a CT domain, inhibited Col I linearization by preventing WISP1-Col I binding. Analysis of patient data revealed that *WISP2* expression is lower in most solid tumors, in comparison to normal tissues. Consequently, genetic or pharmacological restoration of higher WISP2 levels impaired collagen linearization and prevented tumor cell invasion and metastasis *in vivo* in models of human and murine breast cancer. Thus, this study uncovers WISP2 as the first inhibitor of collagen linearization ever identified and reveals that collagen architecture can be normalized and metastasis inhibited by therapeutically restoring a high WISP2:WISP1 ratio.

Keywords

Cancer metastasis; Collagen remodeling; Extracellular matrix; Matricellular proteins; Breast cancer

[*]**Corresponding Author:** Myriam Labelle, St. Jude Children's Research Hospital, 262 Danny Thomas Place, Memphis, TN 38105, Phone: (901) 595-3708, Fax: (901) 595-2270, myriam.labelle@stjude.org.

AUTHORS' CONTRIBUTIONS

J.J., G.P., R.W., B.M.B., H.B.J., E.B., G.C., C.G., and M.L. conducted experiments and acquired data. J.J., G.P., R.W., B.M.B., G.C., C.G., A.S., and M.L. analyzed data. A.M.Z. performed AFM and analyzed the related data. D.F. analyzed RNA-seq data. M.L. wrote the manuscript with input from all coauthors. M.L. supervised the project.

Conflict of interest: The authors declare no potential conflicts of interest.

INTRODUCTION

Metastasis accounts for the vast majority of cancer-related deaths but its underlying mechanisms are not completely understood. During tumor progression, extensive remodeling of the tumor microenvironment occurs and facilitates metastasis (1, 2). In particular, linearization of collagen, one of the most abundant extracellular matrix proteins in solid tumors (3, 4), is recognized as a hallmark of aggressive cancers and is associated with an increased risk of metastasis and poor survival (5).

At the cellular level, linearized collagen facilitates tumor cell invasion and metastasis by providing tracks on which tumor cells can easily migrate (6–12). Therefore, preventing collagen linearization may be a valuable therapeutic approach to limit metastasis (1, 2). However, limited knowledge of the cellular and molecular mechanisms that govern collagen linearization has impeded the development of such therapies. Historically, cell-generated mechanical tension has been proposed to play a role in collagen linearization (13). However, a direct evaluation of its contribution to the organization of Col I in solid tumors is still lacking due to the difficulty of precisely targeting cell-generated mechanical forces without affecting other cellular functions. Therefore, there is a pressing need to identify druggable processes to prevent Col I linearization and metastasis.

We have recently identified a novel mechanism of Col I linearization that is independent of cell-generated mechanical forces and that is based on the secreted matricellular protein WISP1 (14). WISP1 (CCN4) is a TGFβ1-induced cell-secreted factor that binds to Col I and promotes Col I linearization independently of cell-generated mechanical forces (14). Knockdown of WISP1 in cancer cells reduces collagen linearization and inhibits tumor cell invasion and metastasis (14). Thus, collagen linearization is modulated by WISP1 in tumors, either independently or in concert with cell-generated mechanical forces (13, 14). However, a key outstanding question is whether there are molecular antagonists of WISP1 that would actively prevent collagen linearization in normal tissues and that are dysregulated in tumors.

WISP1 is part of a family of structurally related proteins that includes WISP2 (CCN5). These two proteins share three domains, which are 73% homologous between WISP1 and WISP2: an insulin-like growth factor binding protein-like module (IGFBP), a von Willebrand factor type C repeat module (vWC), and a thrombospondin type-1 repeat module (TSP-1). In addition, WISP1 contains a cysteine-rich knot-like C-terminal domain (CT domain) but this domain is absent in WISP2 (15). Whereas high *WISP1* expression in tumors is indicative of poor prognosis (14, 16, 17), high *WISP2* levels correlate with good prognosis in breast cancer patients (18). Altogether, the lack of a CT domain and a prognosis significance that inversely correlates with that of WISP1 suggest that WISP2 could work opposite to WISP1 in regulating collagen linearization and cancer cell metastasis. Here, we have tested this hypothesis and found that WISP2 is an endogenous inhibitor of collagen linearization that has therapeutic potential for impeding cancer progression and metastasis. On this basis, we propose a conceptually novel model whereby pro-metastatic collagen linearization is controlled by the relative bioavailability of two secreted factors with opposing function, WISP1 and WISP2.

MATERIALS AND METHODS

Tissue culture

The 4T1 (ATCC Cat# CRL-2539, RRID:CVCL_0125) murine breast cancer cell line was cultivated in RPMI (Thermo Fisher Scientific Cat# 11875119), 10% FCS (Thermo Fisher Scientific Cat# 10438026), 1% penicillin/streptomycin (Thermo Fisher Scientific Cat# 15140112). The MDA-MB-231 human breast cancer cell line (ATCC Cat# HTB-26, RRID:CVCL_0062) and the 293FT cell line (ATCC Cat# PTA-5077, RRID:CVCL_6911) were cultivated in DMEM (Thermo Fisher Scientific Cat# 11965118), 10% FCS, 1% penicillin/streptomycin. Cells were negative for *Mycoplasma* (last tested in June 2021) and used at passage 2 to 15 after thawing.

Scanning electron microscopy

To prepare collagen solutions, Col I in 0.01 N HCl (PureCol [atelo-type I collagen], Advanced Biomatrix Cat# 5005) or telo-Col I (RatCol [telo-type I collagen], Advanced Biomatrix Cat# 5153) was neutralized (to pH 7.0±0.2) on ice by adding 0.1 M NaOH and mixed with 10X PBS to yield a stock solution containing 2 mg/mL (~6.67 μM) collagen in 1X PBS. Recombinant murine WISP1 (R and D systems Cat# 1680-WS) in PBS or recombinant human WISP2 (PeproTech Cat# 120-16) were added at a final concentration of 50 μg/mL and 100 μg/mL respectively, unless otherwise indicated. The pH of the final collagen + analyte solutions was measured with an Orion PerpHecT ROSS Combination pH Micro Electrode (Thermo Fisher Scientific) and was confirmed to be constant across conditions. 50 μL of collagen solution was transferred to a 16-well glass slide (Thermo Fisher Scientific) and incubated at 37°C for 4h (Col I) or at room temperature for 2 h (telo-Col I) to allow for fibril formation. Collagen lattices were then processed and imaged by scanning electron microscopy as previously described (14) (see also Supplementary Materials and Methods). For each image, the curvature ratio of the collagen fibrils was determined with NIH ImageJ (ImageJ, RRID:SCR_003070) and the numbers of “hairpin- or end-like” structures (fibrils that end or that form sharp bends at angles of 45° or less) and of “knot-like” structures (areas of tangled fibrils) counted in each 72 μm^2 image as described in (14) and in the Supplementary Materials and Methods.

Solid-phase binding assay

For detection of binding to Col I, Col I solution was prepared on ice as described above for scanning electron microscopy. 100 μL of Col I solution were coated in 96-well plates for 10 min at 4 °C. Excess Col I was then removed, and coated plates were incubated at 37°C for 4h to allow for fibril formation. For detection of WISP1-WISP2 binding, plates were coated with 50 μL of 500 nM WISP2 in PBS, 0.01% Tween-20 and incubated overnight at 4°C. The wells were blocked with 2% BSA (GoldBio Cat# A-420-1) in PBS overnight to prevent non-specific binding. Different concentrations of WISP1 and/or WISP2 proteins were prepared in PBS, 1% BSA, incubated on a rotator at room temperature for 45 min, and added to the collagen-coated wells in a 96-well plate, which was then incubated for 2 h at 37°C. For the binding assays with prebound WISP1-Col I or WISP2-Col I complexes, 3 washes with 1X wash buffer (from R and D Systems Cat# DY008) were performed, different concentrations of WISP1 or WISP2 in PBS, 1% BSA were added, and the plate was incubated for 2 h

at 37°C. After 3 additional washes, bound proteins were detected by adding horseradish peroxidase (HRP)-conjugated anti-WISP1 antibody (from the mouse WISP1 Quantikine ELISA Kit, R and D Systems Cat# MWSP10) or with anti-human WISP2 (Thermo Fisher Scientific Cat# PA5-77219, RRID:AB_2720946) followed by HRP-conjugated anti-rabbit IgG (Cell Signaling Technology Cat# 7074, RRID:AB_2099233) in 1X reagent diluent (from R and D Systems Cat# DY008) and incubated for 2 h at room temperature. Plates were then washed 4 times with 1X wash buffer and 100 μL of substrate solution (from R and D Systems Cat# DY008) was added. To stop the reaction, 100 μL of stop solution (from R and D Systems Cat# DY008) was added to each well and the optical density was read at 450 nm (with wavelength correction at 540 nm) with an Infinite M200Pro plate reader and i-control 1.10 software.

Mouse models of breast cancer progression and metastasis

For primary tumor growth and spontaneous metastasis, 8 to 12-week-old syngeneic wild-type BALB/c (Taconic Cat# BALB, RRID:IMSR_TAC:balb) or NSG female mice (The Jackson Laboratory Cat# 005557, RRID:IMSR_JAX:005557) were randomized and anesthetized with isoflurane, and 10^6 tumor cells resuspended in 200 μL HBSS were injected into the 4th mammary fat pad. Mice were euthanized 28 days (4T1) or 70 days (MDA-MB-231) later with CO_2. Tissues were then processed and the tumor weight and numbers of spontaneous lung metastases per mm^2 of lung tissue determined as described in (14) and in Supplementary Materials and Methods. All mice were housed and handled in accordance with approved St. Jude Children's Research Hospital Institutional Animal Care and Use Committee protocols.

Data mining

WISP1 and *WISP2* gene expression levels in cancer patients and adjacent normal tissues were from the GSE62944 data set, which includes RNA-Seq data for 9264 tumor samples and 741 normal samples across 24 cancer types from The Cancer Genome Atlas (TCGA). Breast cancer subtypes were assigned based on the publicly available clinical data for the samples in GSE62944 ("nationwidechildrens.org_clinical_patient_brca" file from https://tcga-data.nci.nih.gov/publications/tcga). Only solid tumor types with TPM data available for at least 3 samples for both the normal and tumor samples were analyzed. Log2(TPM+1) was plotted for *WISP1* and *WISP2* gene expression levels. For the *WISP2/WISP1* ratio, $Log2(TPM_{WISP2}+1/TPM_{WISP1}+1)$ was plotted.

Statistical analysis

Statistics were performed with the GraphPad Prism 8 software (RRID:SCR_002798). Unpaired two-sided *t*-test with Welch's correction was used to compare the means of two independent groups of normally distributed data. If data was not normally distributed, the Mann-Whitney test was used to compare the means of two independent groups. One-way ANOVA followed by Tukey's posttest was used to compare the means of more than two independent groups of normally distributed data.

Data availability

RNA-seq data sets generated and/or analyzed during this study are available at the GEO with accession numbers GSE152514, GSE110912 and GSE62944.

Additional methods (Generation of stable cell lines, Preparation of conditioned medium from stable cell lines, ELISAs, Time-lapse migration assay, Invasion and migration assays, Proliferation assay, RNA-seq, RT-qPCR analysis, Immunoblotting, Picrosirius red staining and polarized light microscopy, Second harmonic generation microscopy, Immunofluorescence staining, Atomic force microscopy) were performed essentially as described previously (14) and are also available in the Supplementary Materials and Methods. DNA, primers, and gRNA sequences used for cloning are also provided (Supplementary Tables S1, S2 and S3).

RESULTS

WISP2 inhibits WISP1-induced collagen linearization.

To determine whether WISP2 directly affects collagen remodeling, we examined the influence of recombinant WISP2 on Col I (PureCol atelo-collagen) architecture in vitro by scanning electron microscopy. These experiments revealed that, in contrast to WISP1, which is sufficient to promote Col I linearization (Fig. 1A and B, Supplementary Fig. S1A and B, and (14)), addition of WISP2 to Col I does not induce any changes in collagen architecture or fibril diameter (Fig. 1A and B, and Supplementary Fig. S1A–C). However, addition of WISP2 in combination with WISP1 (in a 1:3 WISP1:WISP2 molar ratio) results in the formation of Col I lattices that have an architecture similar to control Col I lattices (higher fibril curvature ratio and higher density of knot-like and hairpin- or end-like structures; Fig. 1A and B, and Supplementary Fig. S1A–C), indicating that WISP2 inhibits the effect of WISP1 on Col I linearization. Similar results were obtained with telo-Col I, where WISP1-induced fibril linearization and organization into larger and more linear bundles (14) is inhibited by WISP2 (Supplementary Fig. S1D–F). These findings suggest that the inhibitory effect of WISP2 on WISP1-induced Col I linearization is independent of the presence of collagen telopeptides. On this basis, considering that WISP1 directly binds to Col I (14), WISP2 may inhibit WISP1 by preventing its interaction with Col I.

To test whether WISP2 can disrupt WISP1-Col I interactions, solid-phase binding assays were performed. Results from these assays revealed that both WISP1 and WISP2 have the capacity to bind to fibrillar Col I (Fig. 1C and D). Interestingly, addition of WISP2 to WISP1 (premixed in solution at a 1:3 WISP1:WISP2 molar ratio) inhibits the subsequent binding of WISP1 to Col I (Fig. 1E), but does not interfere with the ability of anti-WISP1 antibodies to bind to WISP1 (Supplementary Fig. S1G), indicating that WISP2 inhibits WISP1's function by preventing WISP1 binding to Col I. Furthermore, combining WISP1 and WISP2 at a 1:1 molar ratio induces a partial inhibition of WISP1-Col I binding (Fig. 1E) and of Col I linearization (Supplementary Fig. S1H–L), indicating that the effect of WISP2 is dose-dependent. In contrast, addition of an excess of WISP1 or WISP2 to prebound WISP1- or WISP2-Col I complexes does not disrupt these interactions (Fig. 1F and G). Since WISP1 and WISP2 are also able to bind to each other (Fig. 1H), these data suggest

that WISP2-WISP1 binding might prevent WISP1-Col I interactions and be a possible mechanism by which WISP2 inhibits WISP1's function. However, this model does not exclude the possibility that free WISP1 and WISP2 also compete for Col I binding sites, and it is conceivable that these two regulatory mechanisms coexist depending on the relative bioavailability of Col I, WISP1, and WISP2 in a specific context. Thus, taken together, these data establish WISP2 as an inhibitor of WISP1 that prevents WISP1-induced Col I linearization. Furthermore, since linearized collagen is more abundant in tumors than in normal tissues (1, 13), these findings suggest that upregulation of *WISP1* versus *WISP2* expression in tumors may drive Col I linearization.

In contrast to *WISP1, WISP2* expression is lower in human solid tumors than in normal tissues.

Mining of publicly available RNA-seq data sets revealed that *WISP2* expression is downregulated in a wide range of solid tumors, including breast, colon, lung, prostate and rectal cancers, in comparison to the corresponding normal tissues (Fig. 2A and Supplementary Fig. S2A). Conversely, consistent with previous studies (19, 20), *WISP1* expression is typically higher in tumors than in normal tissues (Fig. 2B and Supplementary Fig. S2B). The *WISP2*:*WISP1* ratio is therefore generally lower in tumors than in normal tissues (Fig. 2C and Supplementary Fig. S2C). Similar results were also obtained across the four breast cancer subtypes (Luminal A, Luminal B, HER2-enriched and triple-negative), revealing that *WISP2* downregulation and a low *WISP2:WISP1* ratio (<1) occur in a majority of breast tumors, regardless of the subtype (Supplementary Fig. S2D–G). Furthermore, whereas WISP2 is expressed (TPM>1) in 100% of normal tissues adjacent to breast cancers, ~40% of breast tumors express no or very low WISP2 (TPM<1; Supplementary Fig. S2H). Taken together, these results suggest that higher levels of functional WISP1 are found in tumors and that restoration of WISP2 to the levels found in normal tissues might provide a therapeutic intervention that inhibits collagen linearization and consequent tumor cell invasion and metastasis of aggressive tumor cells.

WISP2 inhibits WISP1-induced tumor cell invasion through Col I.

Given that both in vivo and in vitro studies have shown that tumor cells migrate more rapidly onto linearized collagen than onto "normal" disorganized fibrils (6–12), we tested whether addition of recombinant WISP2 inhibits the invasion of triple-negative 4T1 breast cancer cells through Col I. For these studies, 4T1 cells were chosen as the main experimental model because *Wisp1* or *Wisp2* overexpression does not induce any significant gene expression changes in these cells (Supplementary Fig. S2I and (14)). Thus, this cell line provides an ideal system to probe directly how WISP1/2-induced changes in Col I architecture impact tumor cell invasion, independently of alterations in gene expression.

To determine the impact of recombinant WISP1 and WISP2 on cell motility on Col I lattices, time-lapse video microscopy was performed. These studies indicated that the migration speed of 4T1 cells is enhanced on Col I lattices formed in the presence of WISP1 in comparison to control lattices but remains unchanged if lattices are formed in the presence of WISP2 (Fig. 2D and E). Interestingly, 4T1 cells plated on Col I lattices formed in the presence of both WISP1 and WISP2 also fail to migrate faster than cells

plated on control Col I lattices (Fig. 2D and E). These findings indicate that, consistent with its role in inhibiting WISP1-induced Col I linearization, WISP2 prevents increased cell motility on Col I induced by WISP1. Importantly, addition of neither WISP1 nor WISP2 significantly impacts cell motility on plastic surfaces (Fig. 2F and G), further emphasizing a requirement for Col I in WISP1 and WISP2 function. Consistent with time-lapse video microscopy data, WISP2 inhibited WISP1-induced 4T1 cell invasion through Transwells coated with Col I lattices (either atelo- or telo-Col I; Fig. 2H and Supplementary Fig. S2J), in a dose-dependent manner (Supplementary Fig. S2K). However, neither cell migration through uncoated Transwells (Fig. 2I) nor cell proliferation rates were affected (Fig. 2J and Supplementary Fig. S2L and M). Furthermore, WISP1 and WISP2 induced similar effects on the invasion, migration and proliferation of the human triple-negative breast cancer (TNBC) cell line MDA-MB-231 (Fig. 2K–M, and Supplementary Fig. S2N). Taken together, these results indicate that WISP2 inhibits WISP1-induced cell invasion. Given that these results mirror those obtained for collagen remodeling – and since motility on plastic remains unaffected – these data indicate that the effect of WISP1 on cell motility and the inhibitory effect of WISP2 stem from their effects on Col I linearization.

The C-terminal domain of WISP1 is necessary for WISP1-mediated cell invasion.

Our data indicate that both WISP1 and WISP2 bind to Col I, but that only WISP1 is able to induce Col I linearization and to enhance cell invasion (Figs. 1 and 2). WISP2 shares 73% sequence similarity with WISP1, but notably lacks a cysteine-rich C-terminal (CT) domain (Fig. 3A), raising the possibility that the CT domain of WISP1 is responsible for Col I linearization. To understand whether the inhibitory function of WISP2 is indeed due to its lack of a CT domain, we asked whether adding the CT-domain of WISP1 to WISP2 (WISP2+CT) would confer WISP2 the ability to promote Col I linearization and cell invasion and, conversely, whether a form of WISP1 lacking a CT-domain (Wisp1ΔCT) would block the function of WISP1. To this end, overexpression constructs were generated (Fig. 3A) and stably transduced into 4T1 cells (Supplementary Fig. S3A–C). Solid-phase binding assays performed with conditioned medium from WISP1, WISP1ΔCT, WISP2 and WISP2+CT overexpressing cells (Supplementary Fig. S3C) indicated that these protein variants all interact with Col I (Fig. 3B). At equal concentrations, the binding of WISP1ΔCT to Col I was ~75% that of WISP1, suggesting that the CT domain of WISP1, while not required for WISP1-Col I binding, might contribute to facilitating WISP1-Col I interaction (Fig. 3B). However, addition of the CT domain of WISP1 to WISP2 did not further enhance WISP2 binding to Col I (Fig. 3B). Furthermore, coincubation of conditioned media from cells overexpressing non-tagged WISP constructs (i.e., WISP1, WISP1ΔCT, WISP2 and WISP2+CT) together with Myc-tagged WISP1 (WISP1-myc) inhibited WISP1-myc binding to Col I, as measured by detection of Myc-tagged WISP1 (WISP1-myc) interaction with Col I (Fig. 3C and Supplementary Fig. S3D). Thus, all the WISP protein constructs here studied have the ability to bind to Col I and to inhibit WISP1-Col I binding.

We next examined the architecture of Col I lattices formed in the presence of these protein constructs. In contrast to the general capacity of WISP1 and WISP2 constructs to bind to Col I (Fig. 3B), we find that WISP1 and WISP2+CT induce Col I linearization whereas WISP2 and WISP1ΔCT do not (Fig. 3D and E and Supplementary Fig. S3E–G). In line

with these observations, overexpression of *Wisp1* or *Wisp2+CT* in 4T1 cells enhanced their motility on Col lattices and their ability to invade through Col I-coated Transwells, whereas *Wisp2* or *Wisp1ΔCT* overexpression did not have significant effects in these assays (Fig. 3F and G, and Supplementary Fig. S3H). Furthermore, consistent with our previous findings (14), overexpression of these protein constructs affects neither cell motility on plastic nor migration through Transwells (Fig. 3H and I, and Supplementary Fig. S3I). Taken together, these data indicate that the CT domain of WISP1 is dispensable for Col I binding but required for the functional effects of WISP1 on Col I linearization and tumor cell invasion. In addition, these data indicate that WISP2 inhibits the function of WISP1 by preventing its binding to Col I.

WISP2 and WISP1ΔCT block TGFβ1-induced cell invasion through Col I by acting as WISP1 antagonists.

Having established the inhibitory role of WISP2 on tumor cell invasion, we next tested whether its inhibitory function holds true in a context where *Wisp1* is physiologically induced. In 4T1 tumors, *Wisp1* and *Wisp2* are expressed at comparable levels by tumor cells and cancer-associated fibroblasts (CAFs), prominent cell types present in tumors and key modulators of ECM remodeling (Supplementary Fig. S4A and B). Furthermore, the expression of *Wisp1* is markedly upregulated in both cell types upon TGFβ1 treatment (Supplementary Fig. S4C). Given that TGFβ1 is abundant in primary tumors, that it promotes cell invasion, and that it is known to induce *WISP1* expression in a number of cancer cell lines including 4T1 and MDA-MB-231 cells (14, 21–25), we tested whether WISP2 or WISP1ΔCT inhibit TGFβ1-induced cancer cell invasion. To this end, 4T1 cells overexpressing *Wisp2* or *Wisp1ΔCT* were treated with 2 ng/mL recombinant TGFβ1 for 24 h. As expected, TGFβ1 increased endogenous *Wisp1* expression regardless of *Wisp2* or *Wisp1ΔCT* levels (Fig. 4A) and led to increased 4T1-EV cell motility on Col I lattices (Fig. 4B). Interestingly, overexpression of *Wisp2* or *Wisp1ΔCT* was sufficient to block TGFβ1-induced motility of 4T1 cells on Col I lattices (Fig. 4B and Supplementary Fig. S5A), as well as invasion towards a chemoattractant (5% FBS) in Transwell invasion assays (Fig. 4C). Furthermore, similar blockade of TGFβ1-induced 4T1 cell motility on Col I and invasion through Col I in Transwell assays were observed when WISP1 levels were reduced by transducing a pool of 5 Wisp1-targeting gRNAs into 4T1 cells expressing inducible Cas9 (4T1-indCas9; Fig. 4D–F, and Supplementary Fig. S5B). However, *Wisp1* knockout failed to block TGFβ1-induced cell motility on plastic (Supplementary Fig. S5C and D) or Transwell migration (Supplementary Fig. S5E) and did not affect cell proliferation (tested in the presence or absence of TGFβ1; Supplementary Fig. S5F). Thus, inhibition of WISP1 via CRISPR/Cas9 knockout or via overexpression of *Wisp2* or *Wisp1ΔCT* is sufficient to prevent TGFβ1-induced cell motility on Col I, which is one of the most abundant extracellular matrix proteins present in breast tumors (3, 4). On this basis, it is plausible that ectopic expression of WISP2 or WISP1ΔCT would limit tumor cell invasion and prevent metastasis in tumors where the TGFβ1-WISP1 axis is activated.

WISP2 and WISP1ΔCT inhibit metastasis in vivo.

To assess whether WISP2 and WISP1ΔCT inhibit breast tumor progression and metastasis, and conversely, whether WISP2+CT promotes it, 4T1 cells with stable overexpression of

these proteins were implanted into the mammary fat pads of syngeneic BALB/c female mice. No significant differences in tumor growth were noted across the different groups, except for the 4T1-Wisp2 tumors, which grew faster than control 4T1-EV tumors (Fig. 5A). However, mice bearing 4T1-Wisp2 or 4T1-Wisp1ΔCT tumors developed significantly fewer lung metastases than mice bearing 4T1-EV tumors (Fig. 5B), whereas more spontaneous metastases were found in the lungs of mice bearing 4T1-Wisp1 or 4T1-Wisp2+CT tumors (Fig. 5B). Examination of primary tumor sections by second harmonic generation microscopy or by polarized light microscopy following staining with picrosirius red revealed that *Wisp1* or *Wisp2+CT* overexpression results in an increase in the frequency of linear collagen fibers in primary tumors, whereas overexpression of *Wisp2* or *Wisp1ΔCT* has an opposite effect (Fig. 5C and D and Supplementary Fig. S6A). Moreover, linear collagen fiber abundance positively correlated with the stiffness of tumor tissues (Young's modulus; Fig. 5E), consistent with the previously reported role of fibrillar collagen in increasing tumor stiffness (8, 26). The diameters of collagen fibers were also, on average, slightly larger in the 4T1-Wisp1 and 4T1-Wisp2+CT tumors (Supplementary Fig. S6B), suggesting that WISP1-induce Col I linearization may promote the bundling of collagen fibrils into the larger-diameter collagen fibers present in tumors. However, total type I collagen deposition in tumors remained unchanged across the experimental groups (Supplementary Fig. S6C and D), indicating that, as proposed by previous studies (5, 10), the abundance of linear fibers in tumors (rather than total collagen deposition) impacts metastasis. Taken together, these results indicate that WISP1 promotes collagen linearization and spontaneous metastasis in a CT domain-dependent manner, whereas, in contrast, collagen linearization and metastasis are inhibited by WISP2, which lacks a CT domain. Thus, administration of recombinant WISP2 may be envisioned as therapeutic intervention to limit collagen linearization and metastasis.

Treatment with recombinant WISP2 inhibits metastasis in vivo.

To test whether treatment with recombinant WISP2 would be a feasible anti-metastatic therapy, 4T1 cells were implanted into the mammary fat pads of syngeneic BALB/c females and mice were treated with PBS or WISP2 (Fig. 5F). These experiments revealed that treatment with recombinant WISP2 does not affect 4T1 primary tumor growth (Fig. 5G) but inhibits spontaneous lung metastasis (Fig. 5H). A decrease in the frequency (Fig. 5I and J and Supplementary Fig. S6E) and in the average diameter (Supplementary Fig. S6F) of linear collagen fibers was also noted in primary tumors of mice treated with WISP2, whereas total type I collagen deposition remained unaffected (Supplementary Fig. S6G and H).

In addition, we tested whether a shorter treatment regimen would be sufficient to inhibit metastasis in aggressive tumors characterized by high levels of WISP1. To this end, mice bearing 4T1-Wisp1 tumors were treated with recombinant WISP2 from day 8 to day 19 post tumor inoculation (Supplementary Fig. S7A), a time frame during which 4T1 tumor cells invade and access the bloodstream (27). These experiments revealed that this treatment regimen does not impact tumor growth but is sufficient to inhibit spontaneous lung metastasis (Supplementary Fig. S7B and C). However, no difference in linearized collagen fiber abundance was observed (Supplementary Fig. S7D and E), likely due to the

delay between the last dose of recombinant WISP2 (on day 19) and tumor resection (on day 28). Indeed, an independent experiment with tumor resection on day 19 revealed a lower abundance of linearized collagen fibers in tumors from mice treated with recombinant WISP2 (Supplementary Fig. S7F–H), whereas average collagen fiber diameters and total type I collagen deposition in tumors remained unaffected (Supplementary Fig. S7I–K).

Taken together, these results thus indicate that targeting WISP1 with recombinant WISP2 may be a valuable therapeutic approach to limit collagen linearization and to impede cancer metastasis.

WISP2 inhibits invasion and metastasis of human breast cancer xenografts.

To further test the relevance of these findings for human disease, we tested whether overexpression of *WISP1* or *WISP2* in the MDA-MB-231 model of triple-negative human breast cancer xenografts (Supplementary Fig. S8A) affects tumor cell invasion and metastasis. Similar to the results obtained with the 4T1 model, overexpression of *WISP1* in MDA-MB-231 cells promoted tumor cell invasion through Col I lattices (Fig. 6A) but did not affect in vitro cell migration (Fig. 6B) or proliferation (Fig. 6C and Supplementary Fig. S8B). Furthermore, upon orthotopic implantation into the mammary fat pad of NSG mice, no differences in tumor sizes were observed when comparing MDA-MB-231 tumors overexpressing *WISP1* or *WISP2* to control tumors (Fig. 6D). However, *WISP1* overexpression in cancer cells promoted collagen linearization in tumors and spontaneous lung metastasis, whereas *WISP2* overexpression inhibited these processes (Fig. 6E–G and Supplementary Fig. S8C). *WISP1* overexpression also led to a slight but statistically significant increase in collagen fiber diameter (Supplementary Fig. S8D), while no difference in Col I deposition was noted across experimental groups (Supplementary Fig. S8E and F). Thus, forced expression of *WISP1* promotes metastasis in a pre-clinical model of human triple-negative breast cancer, whereas WISP2 limits collagen linearization and metastasis. Together with the lower *WISP2*:*WISP1* ratio observed in human tumors in comparison to normal tissues (Fig. 2C), this suggests that therapeutic manipulation of the relative abundance of WISP1 and WISP2 may provide a novel avenue to control collagen linearization and hence limit metastasis of human tumors.

DISCUSSION

Collagen remodeling is a key event in cancer progression and in other processes such as fibrosis and wound healing. In tumors, aberrant collagen linearization promotes metastasis by providing tracks on which cancer cells can easily migrate (6–8, 12). This mechanism of metastasis is particularly important for breast cancers of the triple-negative subtype (TNBC), which often contain high amounts of aligned fibrillar collagen (28), are very aggressive, and against which no efficient therapy is currently available (29).

The secreted factor WISP1 is by itself able to promote collagen linearization, and knockdown of its expression in cancer cells prevents collagen linearization and inhibits tumor cell invasion and metastasis (14). Thus, in concert with cell-generated mechanical forces, WISP1 plays a pivotal role in promoting collagen linearization in vivo. However, despite the identification of WISP1 as a secreted factor that drives collagen linearization,

it remained unknown whether collagen linearization in physiological and pathological processes can also be modulated by an endogenous inhibitor.

The data presented here demonstrate that WISP2 is a naturally occurring inhibitor of WISP1 that blocks WISP1-induced collagen linearization, tumor cell invasion, and metastasis. Interestingly, previous data suggest that WISP1 and WISP2 might also play antagonistic roles in other processes that rely on extensive collagen remodeling, such as wound healing and fibrosis. Indeed, *Wisp1*$^{-/-}$ mice have a reduced ability to repair wounds, and treatment with anti-WISP1 antibodies prevents pulmonary and liver fibrosis (30–32). In contrast, *Wisp2*$^{-/-}$ mice display enhanced cardiac fibrosis, indicating that WISP2 is anti-fibrotic in this context (33).

Mechanistically, our study reveals that WISP2 – which is structurally similar to WISP1 but lacks a CT domain – is able to bind to both Col I and to WISP1. Binding of WISP2 to WISP1 may therefore mask or alter the conformation of a Col I binding site on WISP1, and thereby impede WISP1-Col I binding. In addition, WISP2 may directly compete with free WISP1 for available binding sites on Col I. However, WISP2 is unable to displace prebound WISP1 (and vice versa), suggesting that both proteins bind tightly to Col I. Consistent with this, mutant forms of WISP1 and WISP2 (WISP1ΔCT and WISP2+CT) also bind to Col I, indicating that binding to Col I does not require the presence of a CT domain. In contrast, we show that the CT domain of WISP1 is necessary for collagen linearization: WISP1ΔCT and WISP2 (which also lacks a CT domain) do not promote collagen linearization, cell invasion, and metastasis, whereas addition of the CT domain of WISP1 to WISP2 confers pro-invasive and pro-metastatic properties to WISP2. On this basis, we propose a model whereby the CT-domain of WISP1 is required for Col I linearization but is dispensable for WISP1-Col I interactions.

CT domains similar to the one found in WISP1 are also present in other proteins such as NGF, TGFβ, PDGF, VEGF, CTGF, vWF, and mucins (34–39). Interestingly, it has been shown that the CT domains of these proteins induce their dimerization, a process that is typically necessary for their bioactivity (37, 38, 40, 41). In addition, analyses of the structure and function of the CT domain of vWF revealed that it not only promotes vWF dimerization, but also allows this large protein to sustain hydrodynamic mechanical forces (38, 40). On this basis, we speculate that the dimerization of Col I-bound WISP1 via its CT domain might stabilize Col I structure and drive its linearization.

The inhibitory effect of WISP2 on the function of WISP1 implies that the relative bioavailability of these two matricellular proteins in tumors or in healthy tissues is a key determinant of Col I architecture. A WISP2/WISP1 balance tipped in favor of WISP1 may therefore promote collagen linearization in tumors. In support of this hypothesis, *WISP2* expression is typically downregulated in tumors compared to normal tissues, whereas *WISP1* expression is upregulated, leading to a lower *WISP2*:*WISP1* ratio. Therefore, this suggests that restoration of WISP2 levels to those found in normal tissues might inhibit the function of WISP1 in tumors, prevent collagen linearization, and limit metastasis in cancer patients. As a proof of principle of the therapeutic potential of this approach, this study demonstrates that increasing WISP2 levels via genetic overexpression or

systemic administration (i.p. injections) of recombinant WISP2 into tumor-bearing mice is sufficient to inhibit TNBC metastasis. Thus, breast cancer patients with aggressive tumors characterized by high levels of WISP1 and linearized collagen might benefit from WISP2 treatments.

TGFβ1 is frequently enriched in the microenvironment of metastatic TNBC where it is an important driver of cancer progression, metastasis, and fibrosis (4, 22, 24, 42). For example, TGFβ1 enhances Col I expression and matrix remodeling by cancer-associated fibroblasts and tumor cells. It also promotes tumor cell invasion via the induction of a wide array of downstream effectors (22, 24), including WISP1 (14). Notably, our results indicate that inhibiting WISP1 via WISP2 or WISP1 knockout is sufficient to inhibit TGFβ1-induced cell invasion through Col I lattices. Thus, WISP1-driven collagen remodeling is necessary for efficient TGFβ1-induced cell invasion through Col I. Since WISP2 does not affect cell proliferation, it might specifically inhibit the pro-invasive effect of TGFβ1 without affecting its cytostatic function. In line with this hypothesis, an inhibitory role for WISP2 downstream of TGFβ1 signaling has been proposed in the context of fibrotic deformation of the retinal pigment epithelium, but the mechanism involved has not yet been characterized (43). Furthermore, it has been previously reported that, in poorly aggressive MCF-7 breast cancer cells, WISP2 acts as a transcriptional repressor and inhibits *Tgfbr2* expression (44). However, *WISP2* overexpression did not trigger any significant changes in *Tgfbr2* levels in metastatic 4T1 cells, indicating that regulation of *Tgfbr2* expression is not a major mechanism by which WISP2 inhibits 4T1 cell invasion and metastasis. In fact, neither WISP2 nor WISP1 overexpression triggers any significant gene expression changes in 4T1 cells (Supplementary Fig. S2I and (14)), suggesting that these matricellular proteins do not significantly affect signal transduction pathways that lead to gene expression. Based on these findings and on our observation that recombinant WISP2 is sufficient to prevent WISP1-induced collagen linearization in a cell-free system, we propose that WISP1 and WISP2 regulate tumor cell invasion through their direct effect on Col I architecture, in response to TGFβ1.

Overall, this study reveals that the secreted factors WISP1 and WISP2 antagonistically regulate collagen linearization during tumor progression and metastasis. Pharmacologically tilting the WISP2/WISP1 balance might therefore provide therapeutic avenues to impede collagen linearization and limit the progression of metastasis in cancer patients.

Supplementary Material

Refer to Web version on PubMed Central for supplementary material.

ACKNOWLEDGMENTS

We thank Aaron Pitre, Jennifer Peters and Victoria Frohlich for assistance with time-lapse video microscopy. We thank Camenzind Robinson, Amanda Johnson and Randall Wakefield for assistance with scanning electron microscopy sample processing and imaging. Images were acquired at the Cell & Tissue Imaging Center, which is supported by SJCRH and NCI P30CA021765. We thank Shondra Pruett-Miller and Samuel Peters of St. Jude's Center for Advanced Genome Engineering for designing and assembling the gRNA vectors. This research was supported by the National Cancer Institute of the National Institutes of Health under Award Numbers R01CA245301 (to M. Labelle) and P30CA021765, and by the ALSAC, the fundraising and awareness organization

for St. Jude Children's Research Hospital. The content is solely the responsibility of the authors and does not necessarily represent the official views of the National Institutes of Health.

Financial support:

NCI R01CA245301 (to M.L.), NCI P30CA021765 (St. Jude Core Facilities), and ALSAC (to M.L.).

REFERENCES

1. Lu P, Weaver VM, and Werb Z. The extracellular matrix: a dynamic niche in cancer progression. J Cell Biol. 2012;196(4):395–406. [PubMed: 22351925]
2. Venning FA, Wullkopf L, and Erler JT. Targeting ECM Disrupts Cancer Progression. Front Oncol. 2015;5:224. [PubMed: 26539408]
3. Naba A, Clauser KR, Lamar JM, Carr SA, and Hynes RO. Extracellular matrix signatures of human mammary carcinoma identify novel metastasis promoters. Elife. 2014;3:e01308. [PubMed: 24618895]
4. Kalluri R, and Zeisberg M. Fibroblasts in cancer. Nat Rev Cancer. 2006;6(5):392–401. [PubMed: 16572188]
5. Conklin MW, Eickhoff JC, Riching KM, Pehlke CA, Eliceiri KW, Provenzano PP, et al. Aligned collagen is a prognostic signature for survival in human breast carcinoma. Am J Pathol. 2011;178(3):1221–1232. [PubMed: 21356373]
6. Condeelis J, and Segall JE. Intravital imaging of cell movement in tumours. Nat Rev Cancer. 2003;3(12):921–930. [PubMed: 14737122]
7. Provenzano PP, Eliceiri KW, Campbell JM, Inman DR, White JG, and Keely PJ. Collagen reorganization at the tumor-stromal interface facilitates local invasion. BMC Med. 2006;4(1):38. [PubMed: 17190588]
8. Levental KR, Yu H, Kass L, Lakins JN, Egeblad M, Erler JT, et al. Matrix crosslinking forces tumor progression by enhancing integrin signaling. Cell. 2009;139(5):891–906. [PubMed: 19931152]
9. Kraning-Rush CM, Carey SP, Lampi MC, and Reinhart-King CA. Microfabricated collagen tracks facilitate single cell metastatic invasion in 3D. Integr Biol (Camb). 2013;5(3):606–616. [PubMed: 23388698]
10. Riching KM, Cox BL, Salick MR, Pehlke C, Riching AS, Ponik SM, et al. 3D collagen alignment limits protrusions to enhance breast cancer cell persistence. Biophys J. 2014;107(11):2546–2558. [PubMed: 25468334]
11. Ray A, Slama ZM, Morford RK, Madden SA, and Provenzano PP. Enhanced Directional Migration of Cancer Stem Cells in 3D Aligned Collagen Matrices. Biophys J. 2017;112(5):1023–1036. [PubMed: 28297639]
12. Oudin MJ, Jonas O, Kosciuk T, Broye LC, Guido BC, Wyckoff J, et al. Tumor Cell-Driven Extracellular Matrix Remodeling Drives Haptotaxis during Metastatic Progression. Cancer Discov. 2016;6(5):516–531. [PubMed: 26811325]
13. Butcher DT, Alliston T, and Weaver VM. A tense situation: forcing tumour progression. Nat Rev Cancer. 2009;9(2):108–122. [PubMed: 19165226]
14. Jia H, Janjanam J, Wu SC, Wang R, Pano G, Celestine M, et al. The tumor cell-secreted matricellular protein WISP1 drives pro-metastatic collagen linearization. EMBO J. 2019;38(16):e101302. [PubMed: 31294477]
15. Perbal B CCN proteins: A centralized communication network. J Cell Commun Signal. 2013;7(3):169–177. [PubMed: 23420091]
16. Clausen MJ, Melchers LJ, Mastik MF, Slagter-Menkema L, Groen HJ, van der Laan BF, et al. Identification and validation of WISP1 as an epigenetic regulator of metastasis in oral squamous cell carcinoma. Genes Chromosomes Cancer. 2016;55(1):45–59. [PubMed: 26391330]
17. Wu J, Long Z, Cai H, Du C, Liu X, Yu S, et al. High expression of WISP1 in colon cancer is associated with apoptosis, invasion and poor prognosis. Oncotarget. 2016;7(31):49834–49847. [PubMed: 27409174]

18. Das A, Dhar K, Maity G, Sarkar S, Ghosh A, Haque I, et al. Deficiency of CCN5/WISP-2-Driven Program in breast cancer Promotes Cancer Epithelial cells to mesenchymal stem cells and Breast Cancer growth. Sci Rep. 2017;7(1):1220. [PubMed: 28450698]
19. Chiang KC, Yeh CN, Chung LC, Feng TH, Sun CC, Chen MF, et al. WNT-1 inducible signaling pathway protein-1 enhances growth and tumorigenesis in human breast cancer. Sci Rep. 2015;5:8686. [PubMed: 25732125]
20. Gurbuz I, and Chiquet-Ehrismann R. CCN4/WISP1 (WNT1 inducible signaling pathway protein 1): a focus on its role in cancer. Int J Biochem Cell Biol. 2015;62:142–146. [PubMed: 25794425]
21. Padua D, and Massague J. Roles of TGFbeta in metastasis. Cell Res. 2009;19(1):89–102. [PubMed: 19050696]
22. Calon A, Tauriello DV, and Batlle E. TGF-beta in CAF-mediated tumor growth and metastasis. Semin Cancer Biol. 2014;25:15–22. [PubMed: 24412104]
23. Oft M, Peli J, Rudaz C, Schwarz H, Beug H, and Reichmann E. TGF-beta1 and Ha-Ras collaborate in modulating the phenotypic plasticity and invasiveness of epithelial tumor cells. Genes Dev. 1996;10(19):2462–2477. [PubMed: 8843198]
24. Bierie B, and Moses HL. Tumour microenvironment: TGFbeta: the molecular Jekyll and Hyde of cancer. Nat Rev Cancer. 2006;6(7):506–520. [PubMed: 16794634]
25. Kuo WH, Chang YY, Lai LC, Tsai MH, Hsiao CK, Chang KJ, et al. Molecular characteristics and metastasis predictor genes of triple-negative breast cancer: a clinical study of triple-negative breast carcinomas. PLoS One. 2012;7(9):e45831. [PubMed: 23049873]
26. Riegler J, Labyed Y, Rosenzweig S, Javinal V, Castiglioni A, Dominguez CX, et al. Tumor Elastography and Its Association with Collagen and the Tumor Microenvironment. Clin Cancer Res. 2018;24(18):4455–4467. [PubMed: 29798909]
27. Sasportas LS, Hori SS, Pratx G, and Gambhir SS. Detection and quantitation of circulating tumor cell dynamics by bioluminescence imaging in an orthotopic mammary carcinoma model. PLoS One. 2014;9(9):e105079. [PubMed: 25188396]
28. Acerbi I, Cassereau L, Dean I, Shi Q, Au A, Park C, et al. Human breast cancer invasion and aggression correlates with ECM stiffening and immune cell infiltration. Integr Biol (Camb). 2015;7(10):1120–1134. [PubMed: 25959051]
29. Foulkes WD, Smith IE, and Reis-Filho JS. Triple-negative breast cancer. N Engl J Med. 2010;363(20):1938–1948. [PubMed: 21067385]
30. Ono M, Masaki A, Maeda A, Kilts TM, Hara ES, Komori T, et al. CCN4/WISP1 controls cutaneous wound healing by modulating proliferation, migration and ECM expression in dermal fibroblasts via alpha5beta1 and TNFalpha. Matrix Biol. 2018.
31. Konigshoff M, Kramer M, Balsara N, Wilhelm J, Amarie OV, Jahn A, et al. WNT1-inducible signaling protein-1 mediates pulmonary fibrosis in mice and is upregulated in humans with idiopathic pulmonary fibrosis. J Clin Invest. 2009;119(4):772–787. [PubMed: 19287097]
32. Li X, Chen Y, Ye W, Tao X, Zhu J, Wu S, et al. Blockade of CCN4 attenuates CCl4-induced liver fibrosis. Arch Med Sci. 2015;11(3):647–653. [PubMed: 26170860]
33. Kim J, Joo S, Eom GH, Lee SH, Lee MA, Lee M, et al. CCN5 knockout mice exhibit lipotoxic cardiomyopathy with mild obesity and diabetes. PLoS One. 2018;13(11):e0207228. [PubMed: 30485307]
34. McDonald NQ, Lapatto R, Murray-Rust J, Gunning J, Wlodawer A, and Blundell TL. New protein fold revealed by a 2.3-A resolution crystal structure of nerve growth factor. Nature. 1991;354(6352):411–414. [PubMed: 1956407]
35. Sun PD, and Davies DR. The cystine-knot growth-factor superfamily. Annu Rev Biophys Biomol Struct. 1995;24:269–291. [PubMed: 7663117]
36. McDonald NQ, and Hendrickson WA. A structural superfamily of growth factors containing a cystine knot motif. Cell. 1993;73(3):421–424. [PubMed: 8490958]
37. Iyer S, and Acharya KR. Tying the knot: the cystine signature and molecular-recognition processes of the vascular endothelial growth factor family of angiogenic cytokines. FEBS J. 2011;278(22):4304–4322. [PubMed: 21917115]
38. Zhou YF, and Springer TA. Highly reinforced structure of a C-terminal dimerization domain in von Willebrand factor. Blood. 2014;123(12):1785–1793. [PubMed: 24394662]

39. Vitt UA, Hsu SY, and Hsueh AJ. Evolution and classification of cystine knot-containing hormones and related extracellular signaling molecules. Mol Endocrinol. 2001;15(5):681–694. [PubMed: 11328851]

40. Voorberg J, Fontijn R, Calafat J, Janssen H, van Mourik JA, and Pannekoek H. Assembly and routing of von Willebrand factor variants: the requirements for disulfide-linked dimerization reside within the carboxy-terminal 151 amino acids. J Cell Biol. 1991;113(1):195–205. [PubMed: 2007623]

41. Kaasboll OJ, Gadicherla AK, Wang JH, Monsen VT, Hagelin EMV, Dong MQ, et al. Connective tissue growth factor (CCN2) is a matricellular preproprotein controlled by proteolytic activation. J Biol Chem. 2018;293(46):17953–17970. [PubMed: 30262666]

42. Bhowmick NA, Chytil A, Plieth D, Gorska AE, Dumont N, Shappell S, et al. TGF-beta signaling in fibroblasts modulates the oncogenic potential of adjacent epithelia. Science. 2004;303(5659):848–851. [PubMed: 14764882]

43. Yoon A, Im S, Lee J, Park D, Jo DH, Kim JH, et al. The matricellular protein CCN5 inhibits fibrotic deformation of retinal pigment epithelium. PLoS One. 2018;13(12):e0208897. [PubMed: 30571728]

44. Sabbah M, Prunier C, Ferrand N, Megalophonos V, Lambein K, De Wever O, et al. CCN5, a novel transcriptional repressor of the transforming growth factor beta signaling pathway. Mol Cell Biol. 2011;31(7):1459–1469. [PubMed: 21262769]

SIGNIFICANCE

Two secreted factors, WISP1 and WISP2, antagonistically regulate collagen linearization, and therapeutically increasing the WISP2:WISP1 ratio in tumors limits collagen linearization and inhibits metastasis.

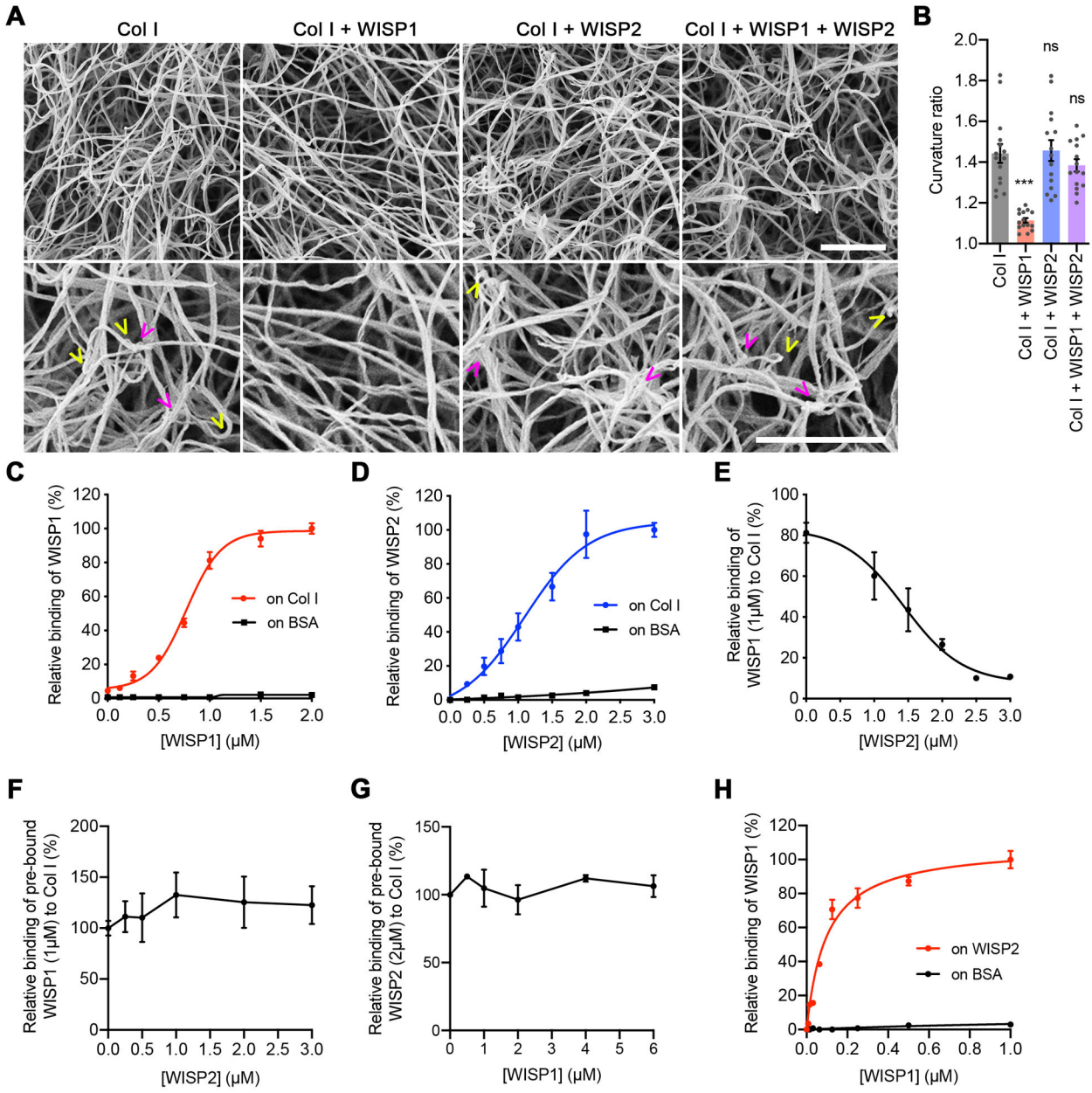

Figure 1. WISP2 inhibits WISP1-induced collagen linearization.

A, Scanning electron microscopy of Col I lattices formed in the presence of PBS (Col I), 50 μg/mL recombinant WISP1, 100 μg/mL recombinant WISP2, or 50 μg/mL WISP1 + 100μg/mL WISP2 (1:3 WISP1:WISP2 molar ratio). Magenta arrows, examples of "knot-like" structures; yellow arrows, examples of "hairpin- or end-like structures". Scale bars, 2 μm.

B, Curvature ratios of Col I fibrils in lattices from **A** (n=15, 3 independent experiments, 5 images/lattice).

C, Binding of WISP1 to fibrillar Col I (or BSA as negative control) as determined by solid-phase binding assay and detected with an anti-WISP1 antibody (n=6, from 3 independent experiments).

D, Binding of WISP2 to fibrillar Col I (or BSA as negative control) as determined by solid-phase binding assay and detected with an anti-WISP2 antibody (n=4, from 2 independent experiments).
E, Inhibition of WISP1 (1 μM) binding to fibrillar Col I in the presence of increasing concentrations of WISP2 (n=6, from 3 independent experiments).
F, Binding of pre-bound WISP1 (1 μM) to fibrillar Col I in the presence of increasing concentrations of WISP2 (n=6, from 3 independent experiments).
G, Binding of pre-bound WISP2 (2 μM) to fibrillar Col I in the presence of increasing concentrations of WISP1 (n=4, from 2 independent experiments).
H, Binding of WISP1 to WISP2 (or BSA as negative control) as determined by solid-phase binding assay (n=4, from 2 independent experiments).
(B-H) mean ± SEM, (B) one-way ANOVA followed by Tukey's posttest. ns, $P>0.05$; ***, $P<0.001$.

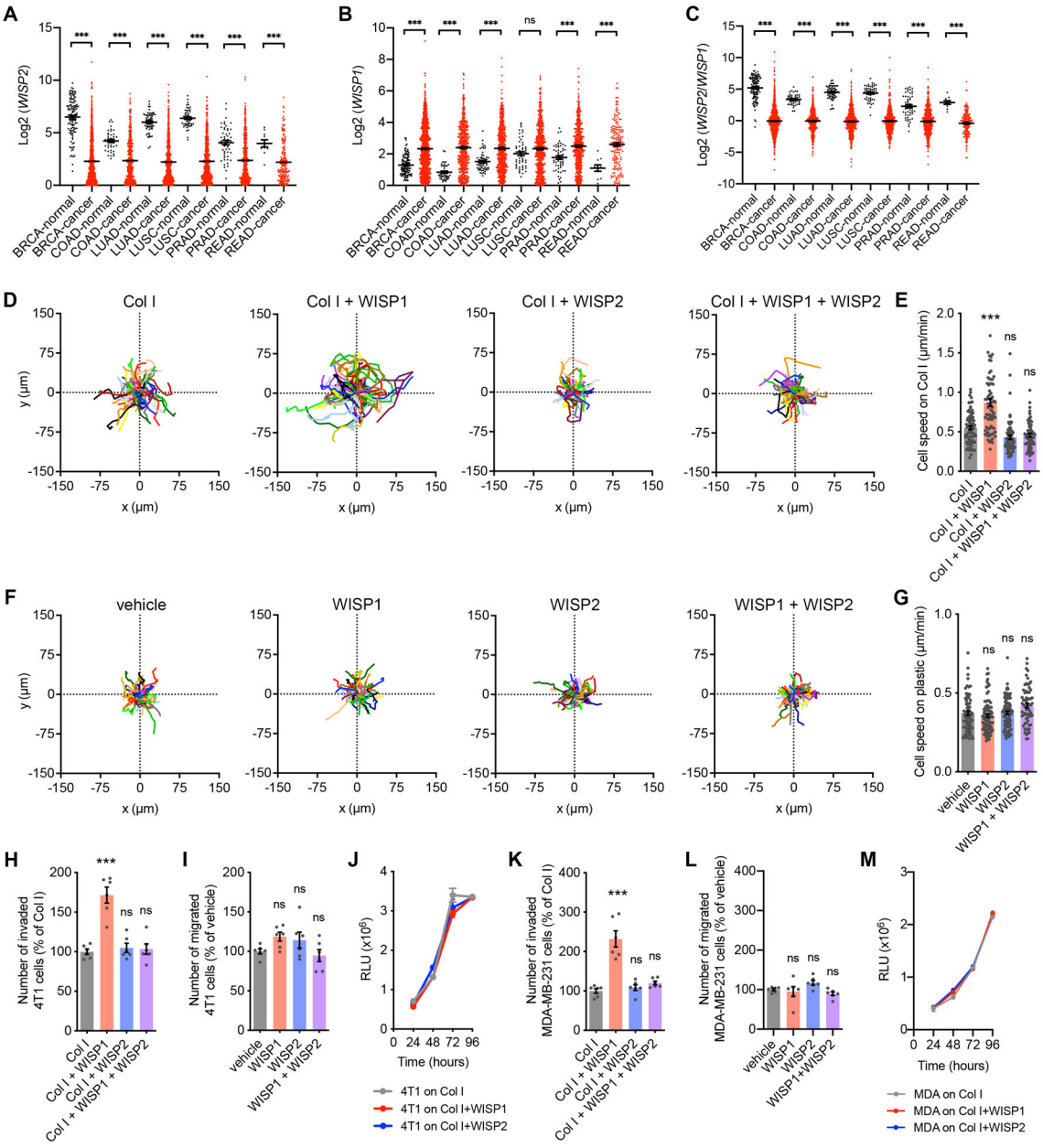

Figure 2. WISP2 inhibits WISP1-induced cell invasion through Col I.

A-C, *WISP2* (**A**) or *WISP1* (**B**) gene expression levels, or *WISP2/WISP1* gene expression ratio (**C**) in tumors and adjacent normal tissues from patients with different cancer types (BRCA, breast invasive carcinoma, n=113 normal and n=1119 tumors; COAD, colon adenocarcinoma, n=41 normal and n=483 tumors; LUAD, lung adenocarcinoma, n=59 normal and n=541 tumors; LUSC, lung squamous cell carcinoma, n=51 normal and n=502 tumors; PRAD, prostate adenocarcinoma, n=52 normal and n=502 tumors; READ, rectum adenocarcinoma, n=10 normal and n=167 tumors).

D, Migratory tracks of 4T1 cells plated on Col I (n=72 cells), Col I + WISP1 (n=77 cells), Col I + WISP2 (n=72 cells), or Col I + WISP1 + WISP2 (n=62 cells) lattices.

E, Average cell speed from cells tracked in **D**.

F, Migratory tracks of 4T1 cells plated on plastic in presence of PBS vehicle control (n=69 cells), WISP1 (n=85 cells), WISP2 (n=81 cells), or WISP1 + WISP2 (n=65 cells).
G, Average cell speed from cells tracked in **F**.
H, Invasion of 4T1 cells through Col I layered on Transwell inserts, in the presence of WISP1, WISP2, or WISP1 + WISP2 (1:3 WISP1:WISP2 molar ratio; n=6 biological replicates).
I, Migration of 4T1 cells through the microporous membrane of Transwell inserts (in the absence of Col I) in the presence of PBS (vehicle), WISP1, WISP2, or WISP1 + WISP2 (n=6 biological replicates).
J, Proliferation rate of 4T1 cells plated on Col I, Col I + WISP1, or Col I + WISP2 lattices (n=4 biological replicates).
K, Invasion of MDA-MB-231 cells through Col I layered on Transwell inserts, in the presence of WISP1, WISP2, or WISP1 + WISP2 (n=6 biological replicates).
L, Migration of MDA-MB-231 cells through the microporous membrane of Transwell inserts (in the absence of Col I) in the presence of PBS (vehicle), WISP1, WISP2, or WISP1 + WISP2 (n=6 biological replicates).
M, Proliferation rate of MDA-MB-231 cells plated on Col I, Col I + WISP1, or Col I + WISP2 lattices (n=4 biological replicates).
(A-C, E, G-M) mean ± SEM, (A-C) Mann-Whitney test, (E, G-I, K, L) one-way ANOVA followed by Tukey's posttest. ns, $P>0.05$; ***, $P<0.001$.

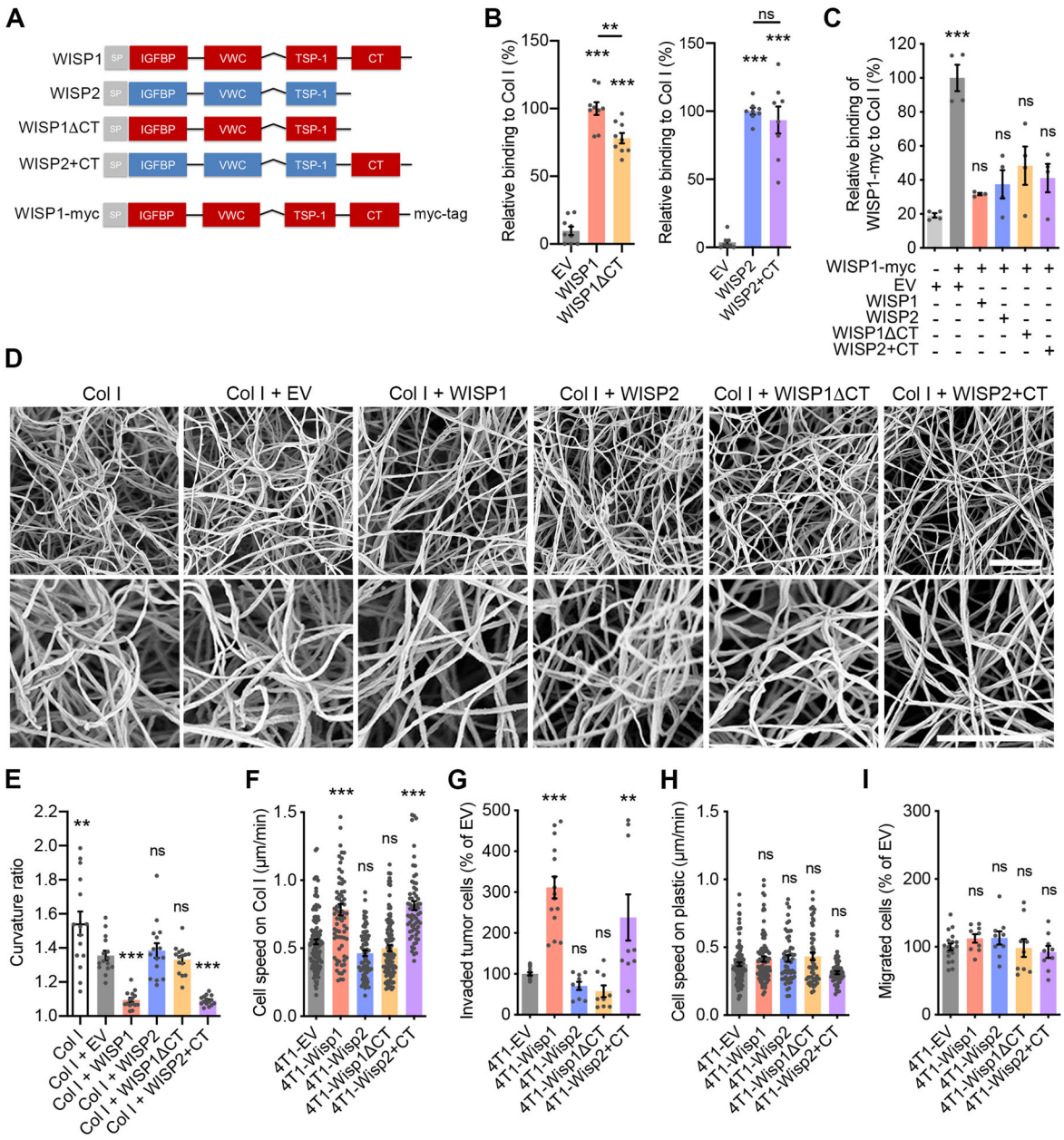

Figure 3. The C-terminal domain of WISP1 drives WISP1-induced Col I linearization and cell invasion but is dispensable for WISP1-Col I binding.

A, Scheme of WISP constructs stably transduced in 4T1 cells. IGFBP, insulin-like growth factor domain; VWC, von Willebrand factor type C repeat domain; TSP-1, thrombospondin type-1 repeat domain; CT, cysteine-rich knot-like C-terminal domain.

B, Detection of WISP1, WISP1ΔCT, WISP2, and WISP2+CT binding to fibrillar Col I, using conditioned media from 4T1 cells stably overexpressing these constructs or stably transduced with an empty vector (EV) control. Col I-bound proteins were detected with anti-WISP1 (left) or anti-WISP2 (right) antibodies. Binding was normalized to the molarity of each construct in the conditioned medium (left, n=9, from 3 independent experiments; right, n=8, from 4 independent experiments).

C, Binding of WISP1-myc protein to fibrillar Col I in the presence of WISP1, WISP2, WISP1ΔCT, or WISP2+CT, using 1:1 (v:v) ratios of conditioned medium from 4T1 cells overexpressing these proteins. Conditioned medium from 4T1-EV (4T1 cells stably transduced with an empty vector) was used as negative control. Col I-bound proteins were detected with an anti-Myc antibody (n=4, from 2 independent experiments).
D, Scanning electron microscopy of Col I lattices formed in the presence of concentrated conditioned medium from 4T1 stable cell lines. Scale bars, 2 μm.
E, Curvature ratios of Col I fibrils in lattices from **D** (n=15, 3 independent experiments, 5 images/lattice). Statistical significance vs Col I + EV is shown.
F, Average cell speed of 4T1-EV (n=123), 4T1-Wisp1 (n=75), 4T1-Wisp2 (n=69), 4T1-Wisp1ΔCT (n=106), and 4T1-Wisp2+CT (n=66) cells plated on Col I lattices.
G, Invasion of 4T1-EV, 4T1-Wisp1, 4T1-Wisp2, 4T1-Wisp1ΔCT, or 4T1-WISP2+CT cells through Col I lattices layered on Transwell inserts (n=9, except 4T1-EV and 4T1-Wisp1, n=15 biological replicates).
H, Average cell speed of 4T1-EV (n=115), 4T1-Wisp1 (n=89), 4T1-Wisp2 (n=54), 4T1-Wisp1ΔCT (n=53), and 4T1-Wisp2+CT (n=59) cells plated on plastic.
I, Migration of 4T1-EV, 4T1-Wisp1, 4T1-Wisp2, 4T1-Wisp1ΔCT, or 4T1-WISP2+CT cells through uncoated Transwell inserts (n=9, except 4T1-EV, n=18 biological replicates).
(B, C, E-I) mean ± SEM, one-way ANOVA followed by Tukey's posttest. ns, $P>0.05$; **, $P<0.01$; ***, $P<0.001$.

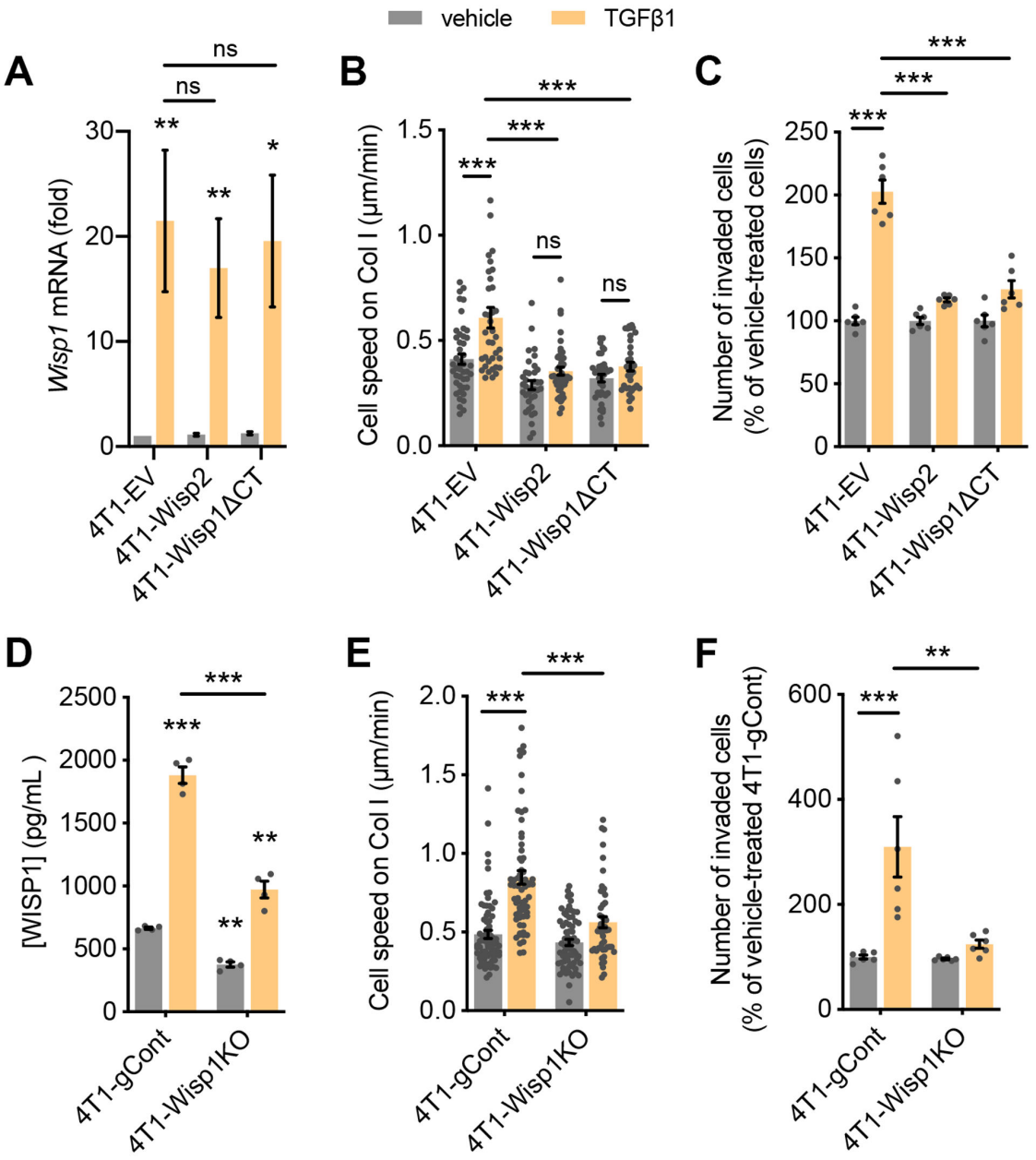

Figure 4. WISP2 and WISP1ΔCT block TGFβ1-induced cell invasion through Col I by acting as WISP1 antagonists.

A, Relative *Wisp1* mRNA expression levels in 4T1-EV (4T1 cells stably transduced with an empty vector), 4T1-Wisp1ΔCT, and 4T1-Wisp2 cells cultured in the presence of vehicle or TGFβ1 (2 ng/mL). Primers targeting sequences coding in the CT domain of *Wisp1* were used to detected endogenous *Wisp1* expression levels but not overexpressed *Wisp1ΔCT* (n=3 biological replicates).

B, Average cell speed of 4T1-EV + vehicle (n=44), 4T1-EV + 2 ng/mL TGFβ1 (n=37), 4T1-Wisp2 + vehicle (n=36), 4T1-Wisp2 cells + TGFβ1 (n=44), 4T1-Wisp1ΔCT + vehicle (n=36), and 4T1-Wisp1ΔCT + TGFβ1 (n=35) cells plated on Col I lattices.

C, Invasion of 4T1-EV, 4T1-Wisp2, and 4T1-Wisp1ΔCT cells treated with TGFβ1 (2 ng/mL) or vehicle control, through Col I lattices layered on Transwell inserts (n=6 biological replicates).

D, WISP1 protein concentration in conditioned medium from 4T1-gCont (4T1-indCas9 cells stably transduced with a pool of control non-targeting gRNAs) and 4T1-Wisp1KO (4T1 cells with CRISPR/Cas9 knockout of *Wisp1*) treated with TGFβ1 (2 ng/mL) or vehicle control (n=4, from 2 independent experiments).

E, Average cell speed of 4T1-gCont + vehicle (n=72), 4T1-gCont + TGFβ1 (n=64), 4T1-Wisp1KO (n=68), 4T1-Wisp1KO + TGFβ1 (n=48) cells plated on Col I lattices.

F, Invasion of 4T1-gCont and 4T1-Wisp1KO cells, treated with TGFβ1 (2 ng/mL) or vehicle control, through Col I lattices layered on Transwell inserts (n=6 biological replicates).

Mean ± SEM, two-way ANOVA followed by Tukey's posttest. ns, $P>0.05$; *, $P<0.05$; **, $P<0.01$; ***, $P<0.001$.

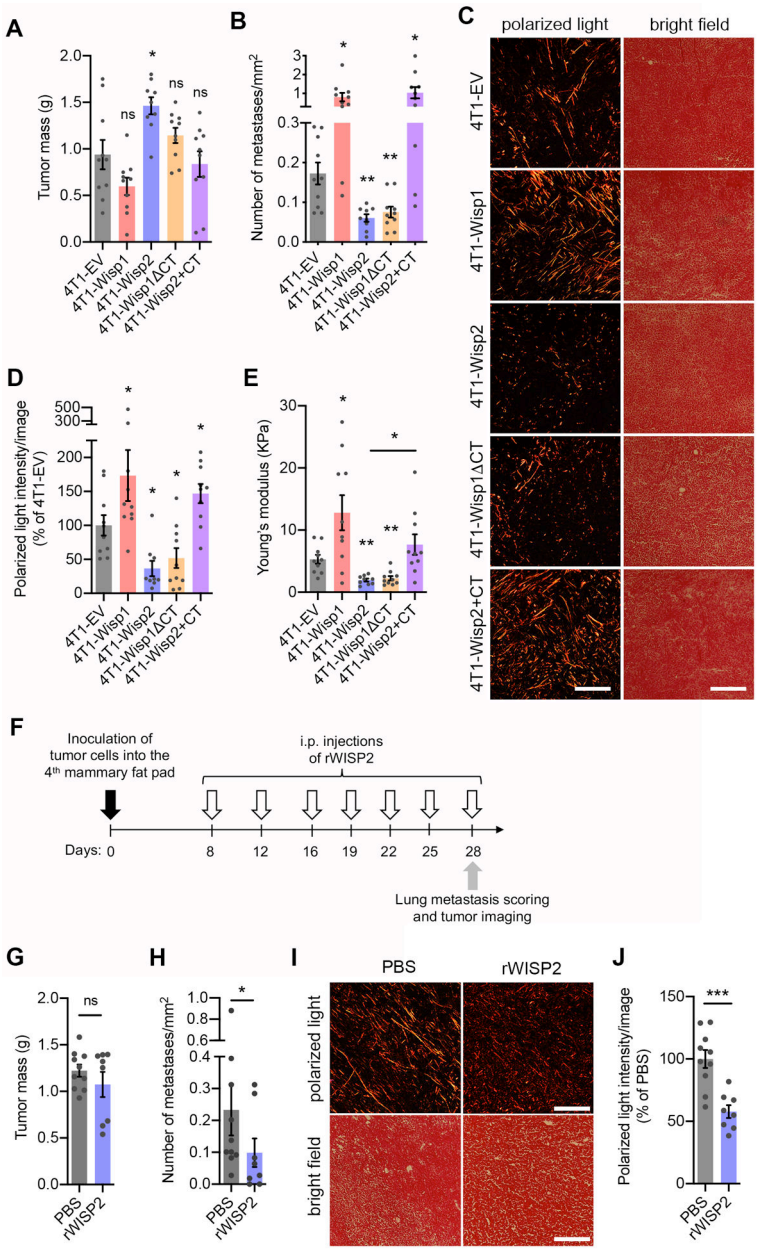

Figure 5. WISP2 limits collagen linearization in tumors and inhibits breast cancer metastasis.

A, Primary tumor mass, 28 days after orthotopic inoculation of 4T1-EV, 4T1-Wisp1, 4T1-Wisp2 or 4T1-Wisp1ΔCT cells into the 4th mammary fat pad of BALB/c female mice (n=10 mice/group, except 4T1-Wisp2, n=9 mice).

B, Numbers of lung metastases in mice from **A**.

C, Representative images of fibrillar collagen in primary tumors from **A** visualized by picrosirius red staining followed by polarized light microscopy. Corresponding bright-field images show tissue integrity. Scale bars, 200 μm.

D, Average polarized light intensity in picrosirius red staining images of tumors from **A**.

E, Average stiffness (Young's modulus) of tumors from **A**, measured by atomic force microscopy.

F, Scheme of experimental design. Recombinant WISP2 (rWISP2; 100 μg in 200 μL PBS) was administered via intraperitoneal injection starting on day 8 post-injection of 4T1 cells. Tissues were collected 2 h after the last dose of rWISP2.

G, Primary tumor mass, 28 days after orthotopic inoculation of 4T1 cells into the 4^{th} mammary fat pad (PBS, n=10; rWISP2, n=8 mice/group).

H, Numbers of lung metastases in mice from **G**.

I, Representative images of fibrillar collagen in primary tumors from **G** visualized by picrosirius red staining followed by polarized light microscopy. Corresponding bright-field images show tissue integrity. Scale bars, 200 μm.

J, Average polarized light intensity in picrosirius red staining images of tumors from **G**. (A, B, D, E, G, H, J) mean ± SEM, (A, B, D, E) one-way ANOVA followed by Tukey's posttest. (G, H, J) unpaired two-sided *t*-test. ns, $P>0.05$; *, $P<0.05$; **, $P<0.01$, ***, $P<0.001$.

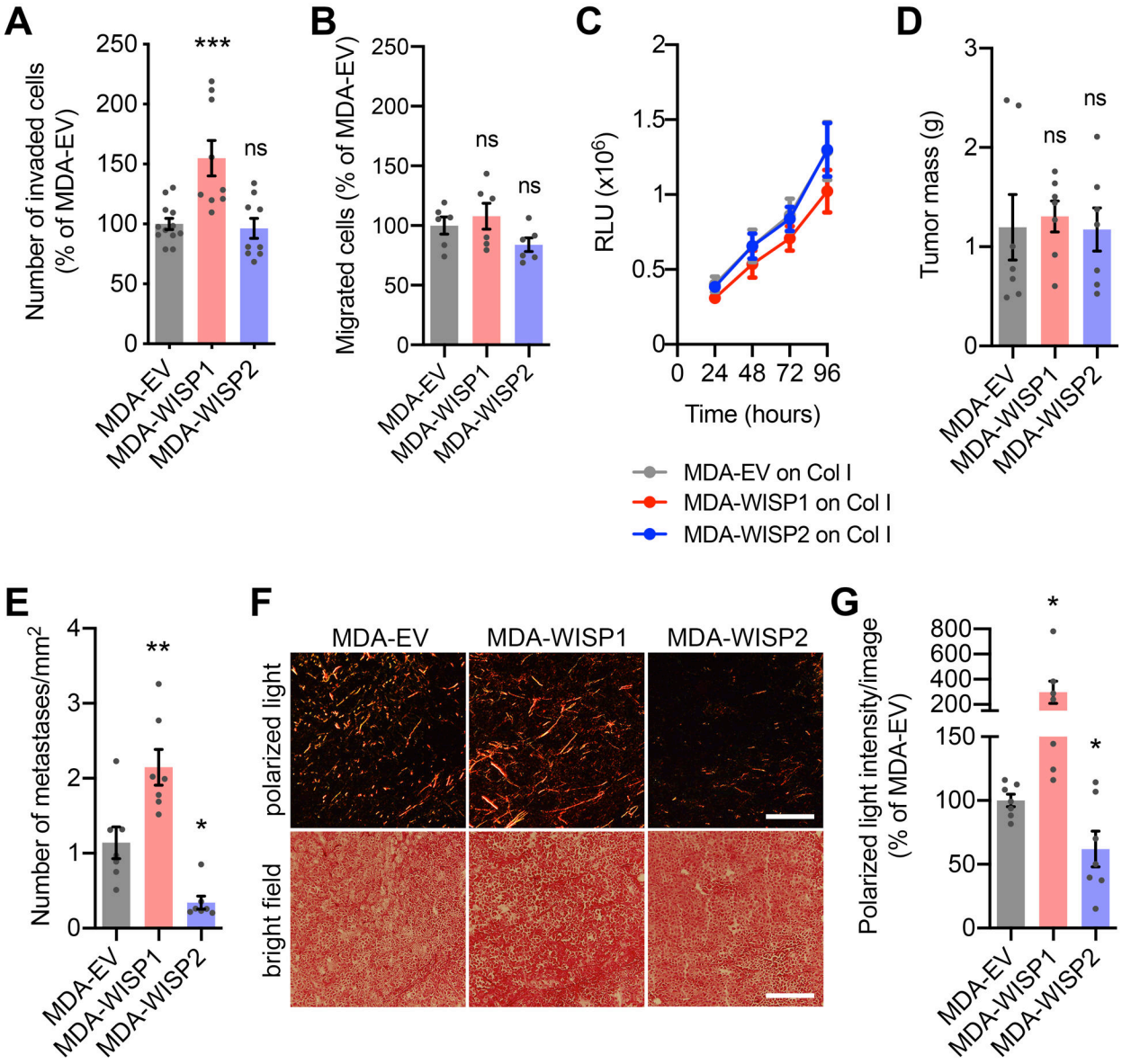

Figure 6. WISP1 promotes whereas WISP2 inhibits human breast cancer metastasis.

A, Invasion of MDA-MB-231 cells overexpressing *WISP1* (MDA-WISP1) or *WISP2* (MDA-WISP2), or stably transduced with an empty vector control (MDA-EV) through Col I lattices layered on Transwell inserts (n=9 biological replicates).

B, Migration of MDA-EV, MDA-WISP1, or MDA-WISP2 cells through uncoated Transwell inserts (n=6 biological replicates).

C, Proliferation rate of MDA-EV, MDA-WISP1, or MDA-WISP2 cells plated on Col I lattices. (n=12 biological replicates).

D, Primary tumor mass, 70 days after orthotopic inoculation of MDA-EV, MDA-WISP1, or MDA-WISP2 cells into the 4th mammary fat pad of NSG female mice (n=7 mice/group).

E, Numbers of lung metastases in mice from **D**.

F, Representative images of fibrillar collagen in primary tumors from **D** visualized by picrosirius red staining followed by polarized light microscopy. Corresponding bright-field images show tissue integrity. Scale bars, 200 μm.

G, Average polarized light intensity in picrosirius red staining images of tumors from **D**. (A-E, G) mean ± SEM, (A, B, D, E, G) one-way ANOVA followed by Tukey's posttest. ns, $P>0.05$; *, $P<0.05$; **, $P<0.01$; ***, $P<0.001$.